Experimental Evaluation of Laser Attenuation
by Water Drops

J. T. Miller
ARO, Inc.

August 1979

Final Report for Period January 2 — September 30, 1978

ARNOLD ENGINEERING DEVELOPMENT CENTER
ARNOLD AIR FORCE STATION, TENNESSEE
AIR FORCE SYSTEMS COMMAND
UNITED STATES AIR FORCE

This report has been reviewed by the Information Office (OI) and is releasable to the National Technical Information Service (NTIS). At NTIS, it will be available to the general public, including foreign nations.
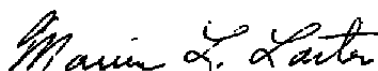
APPROVAL STATEMENT

This report has been reviewed and approved.

MARSHALL K. KINGERY
Project Manager, Research Division
Directorate of Test Engineering

Approved for publication:

FOR THE COMMANDER

MARION L. LASTER
Director of Test Engineering
Deputy for Operations

REPORT DOCUMENTATION PAGE		READ INSTRUCTIONS BEFORE COMPLETING FORM
1. REPORT NUMBER AEDC-TR-79-18	2. GOVT ACCESSION NO.	3. RECIPIENT'S CATALOG NUMBER
4. TITLE (and Subtitle) EXPERIMENTAL EVALUATION OF LASER ATTENUATION BY WATER DROPS		5. TYPE OF REPORT & PERIOD COVERED Final Report – January 2 to September 30, 1978
		6. PERFORMING ORG. REPORT NUMBER
7. AUTHOR(s) J. T. Miller, ARO, Inc., a Sverdrup Corporation Company		8. CONTRACT OR GRANT NUMBER(s)
9. PERFORMING ORGANIZATION NAME AND ADDRESS Arnold Engineering Development Center/DOTR Air Force Systems Command Arnold Air Force Station, TN 37389		10. PROGRAM ELEMENT, PROJECT, TASK AREA & WORK UNIT NUMBERS Program Element 65807F
11. CONTROLLING OFFICE NAME AND ADDRESS Arnold Engineering Development Center/OIS Air Force Systems Command Arnold Air Force Station, TN 37389		12. REPORT DATE August 1979
		13. NUMBER OF PAGES 28
14. MONITORING AGENCY NAME & ADDRESS(if different from Controlling Office)		15. SECURITY CLASS. (of this report) UNCLASSIFIED
		15a. DECLASSIFICATION/DOWNGRADING SCHEDULE N/A

16. DISTRIBUTION STATEMENT (of this Report)

Approved for public release; distribution unlimited.

17. DISTRIBUTION STATEMENT (of the abstract entered in Block 20, if different from Report)

18. SUPPLEMENTARY NOTES

Available in DDC

19. KEY WORDS (Continue on reverse side if necessary and identify by block number)

attenuation   test methods
laser beams
drops
water

20. ABSTRACT (Continue on reverse side if necessary and identify by block number)

A test program was conducted to measure the transmission of both CO_2 and HeNe laser beams through an attenuation region occupied by water drops. Analysis of the measurements shows that there is reasonable agreement between experiment and diffraction theory and that the major source of uncertainty arises from the characterization of the attenuating particle field.

DD FORM 1473 EDITION OF 1 NOV 65 IS OBSOLETE
1 JAN 73

PREFACE

CONTENTS

ILLUSTRATIONS

Figure

TABLES

1.0 INTRODUCTION

Lasers are being used in environments that may have adverse transmission properties. Communications applications, for example, may require that the laser signal be transmitted reliably over long distances that may occasionally be obscured by clouds of rain, dust, or fog.

One important role of laser testing is to define the transmission degradation that adverse environments produce. It is essential that realistic, well-defined test conditions be available for such tests. The purpose of the present test effort was to make transmission measurements for carbon dioxide (CO_2) and helium-neon (HeNe) laser beams attenuated by water drops. An existing AEDC facility and technology developed for other applications were used to obtain the measurements. The approach was to introduce attenuating particles into a laser beam and directly measure the resulting transmission change.

2.0 APPARATUS

2.1 TEST UNIT

The test facility is a 60-ft long, 8-ft-diam steel tank that can be evacuated to any desired pressure between an atmosphere and a few millimeters of mercury (mmHg). The normal test gas is air, but other gases are available. Humidity control is also available, since both a dry air source and a steam line are installed. Liquid-nitrogen plumbing is installed for local cooling inside the tank when required. The experimental arrangement is depicted in Fig. 1, and the general optical arrangement is shown in Fig. 2.

A water drop generator provided the particulate field for the attenuation experiments. Drop size was varied between 0.3 and 1.4 mm. A monodisperse water drop generator was mounted below the coincident laser beams so that the trajectory of the stream of water drops entered the beam and then fell out of the beam as depicted in Fig. 3. The monodisperse generator used is an example of the equipment developed for hypervelocity erosion testing in a ballistics range. In that application, the generator is mounted so that the drops fall vertically into the path of the projectile. For laser attenuation testing, the usual vertical mounting would not place enough drops in the beam to produce appreciable attenuation.

The monodisperse generator employs a vibrating orifice that breaks the water stream into uniformly sized drops. The orifice is vibrated by a piezo-electric crystal, to produce a single drop for each electrical pulse from a signal generator. Thus, the easily measured and

5
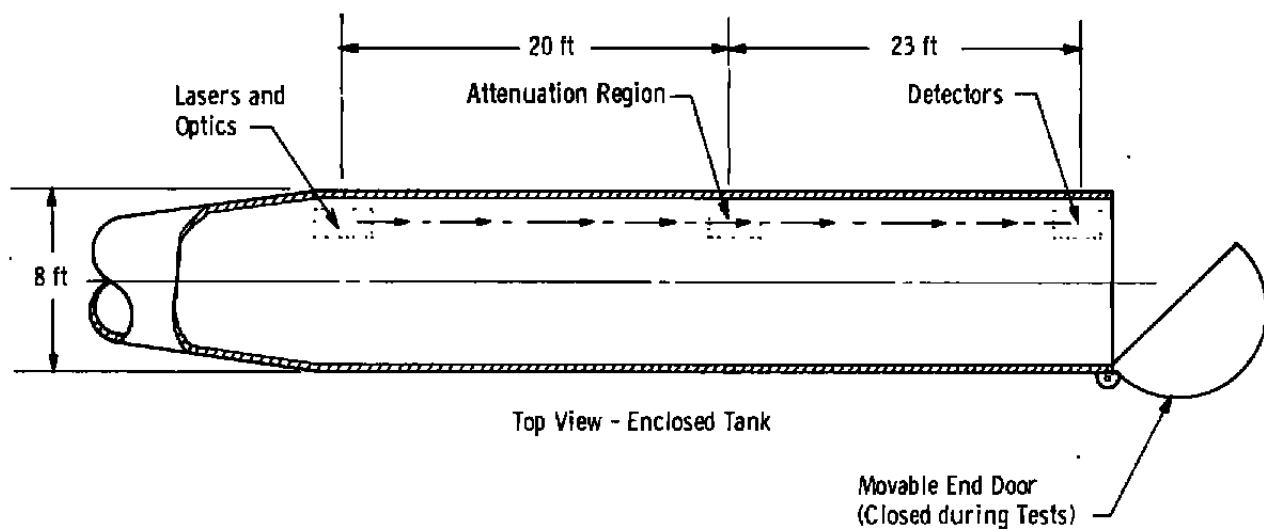
Figure 1. Experimental layout.
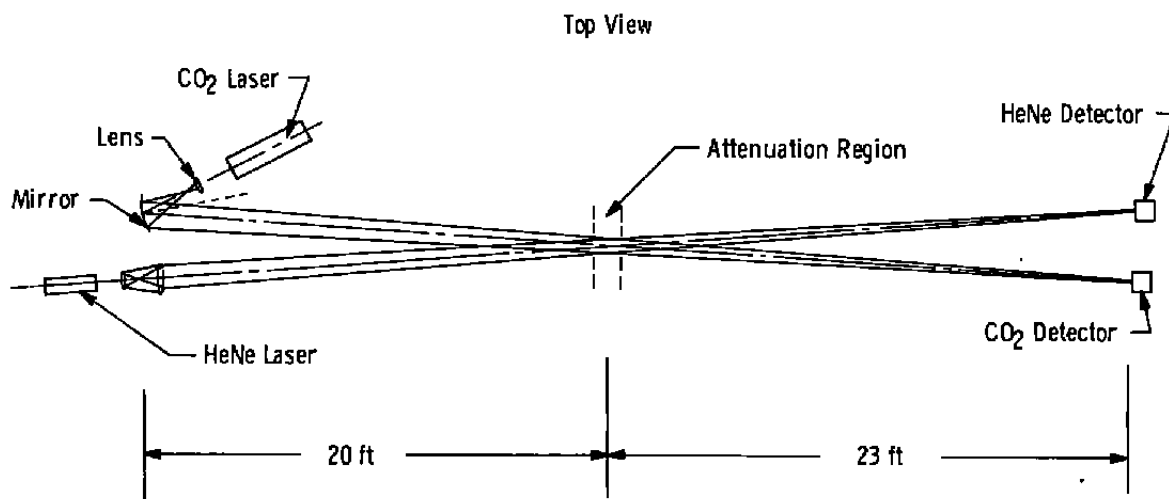
Figure 2. Optical arrangement.

6

controlled signal generator frequency is the drop formation frequency. The water drops have a diameter uniformity of ±2 percent, and the particle diameter can be calculated from the operating conditions of the generator to better than 2-percent accuracy. This experimental arrangement places a stream of water drops into the coincident laser beams, as depicted in Fig. 4, so that the attenuation of each beam by a common collection of water drops can be measured.

2.2 INSTRUMENTATION

A CO_2 laser and an HeNe laser were used for the attenuation experiments. The CO_2 laser was a 3-w continuous device. An attenuator was installed on the laser to reduce the power output to the 1/2-w level. The initial beam was expanded to a 1.7-in. diameter using a germanium lens and was then focused onto the detector at the far end of the tank. This focusing was accomplished by a 6-in.-diam, 48-in.-focal-length, spherical, concave mirror. The beam size at the detector was approximately 1/4 in. in diameter.

The HeNe laser was a 15-mw continuous device. The beam was expanded to a 1.5-in. diameter and then focused onto a detector at the far end of the tank. The expanding and focusing were accomplished using a commerical beam expander attached directly to the laser.

The geometric arrangement is depicted in Fig. 1. A more detailed diagram of the optical arrangement is given in Fig. 2, in which the angle between the two laser beams is greatly exaggerated. An important feature of the arrangement is that the two beams are essentially coincident through the particulate region.

The output of each detector was directed to a minicomputer so that the analog output signals could be digitized online and stored in digital form for subsequent computer processing. The system has the capability to digitize and record both channels for 0.32 sec in real time at a frequency of 3.135 kHz.

Other features of the experimental arrangement included a provision for completely shielding the detectors from the laser beams to establish the zero level output and a provision for blocking the water drops injected into the laser beams so that the full-scale output of the detectors could be established.

7
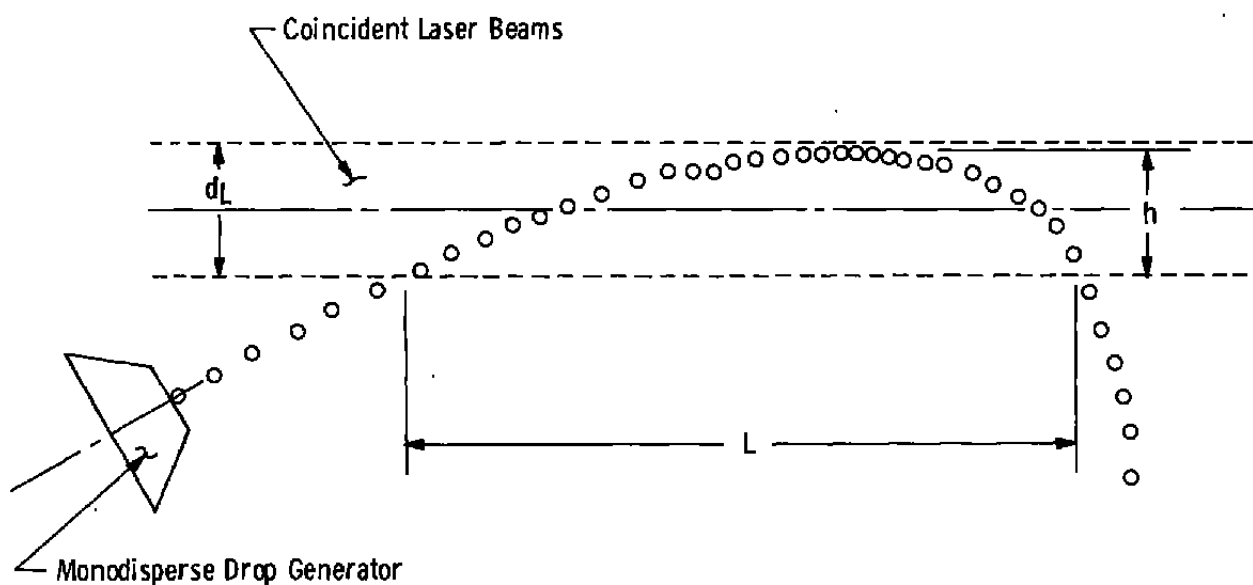
Figure 3.   Particulate region - side view.
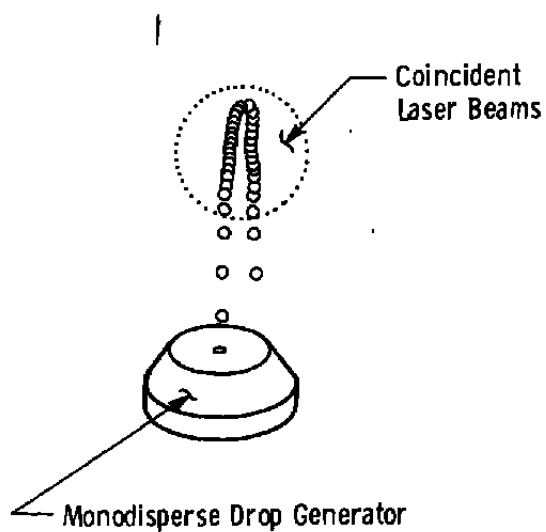
Figure 4.   Particulate region as viewed along laser beam axis.

3.0 PROCEDURE

3.1 EXPERIMENTAL PROCEDURE

Test measurements consisted of direct measurements of the laser attenuation produced by the water drops and measurements needed to define the size and population of attenuating water drops in the laser beams. For each test measurement, the water flow was first established. The water flow rate to the drop generator was measured, as was the frequency of the signal supplied to the drop generator. These quantities gave the drop formation frequency and size. Other measurements included the height of the drop trajectory into the laser beam (h in Fig. 3) and length of the drop trajectory in the laser beam (L in Fig. 3). These quantities, along with the drop formation frequency and the drop size, defined the drop spacing along the trajectory. Some variation existed in the trajectory length along the axis, L. This quantity was also needed to define the cross-sectional area the drops present to the laser beams.

After the flow parameters were measured, the detector outputs, which correspond to no laser signal, were established by completely shielding the detectors from the laser beams. This information was recorded over a 0.32-sec time span, so that the effects of various sources of noise, if they existed, could be averaged out. Once the null-level output was established, the full-scale output was measured in a like manner, by blocking the water flow into the laser beam. An example of the full-scale output recorded for 0.32 sec is shown in Fig. 5.

A test shot was then made during which the outputs of the respective detectors were recorded for 0.32 sec. The test outputs, corresponding to the calibration values shown in Fig. 5, are shown in Fig. 6. Figures 5 and 6 show that the signal from the HeNe detector was relatively uniform, but the signal from the CO_2 detector had a 120-Hz noise component, which apparently was inherent in the laser. The detector outputs were plotted for each test as shown in Figs. 5 and 6. If they appeared to be satisfactory, the data points were recorded on magnetic tape for subsequent computer processing.

3.2 EXPERIMENTAL DATA REDUCTION

The transmission is defined as the ratio of the power transmitted through the attenuation region to that incident on the attenuation region. The experimental transmission is therefore given by

$$T = (V - V_0) / (V_F - V_0) \qquad (1)$$
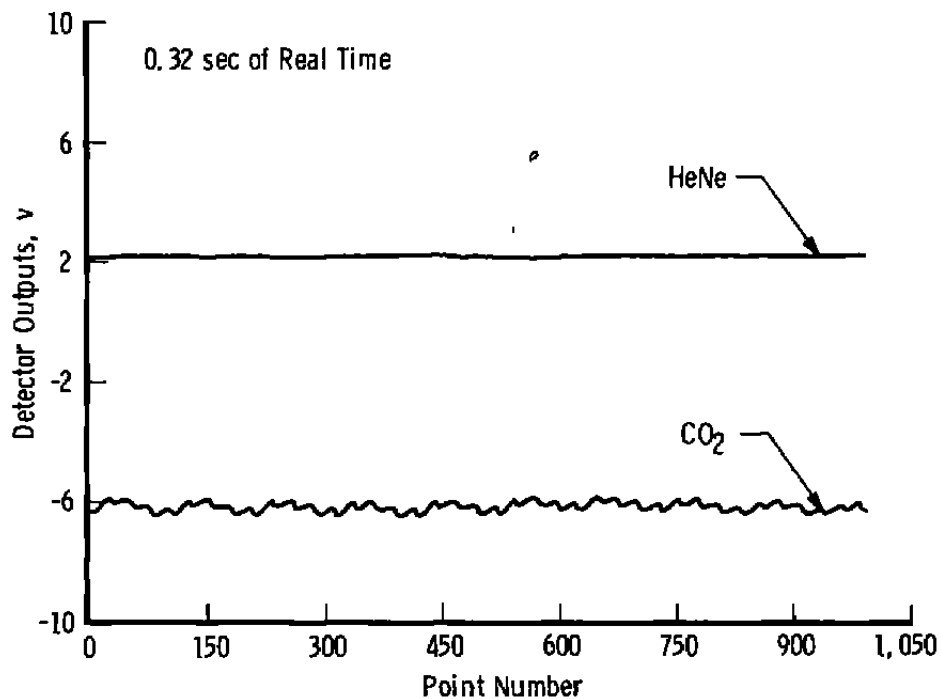
Figure 5. Sample of full-scale output of detectors.
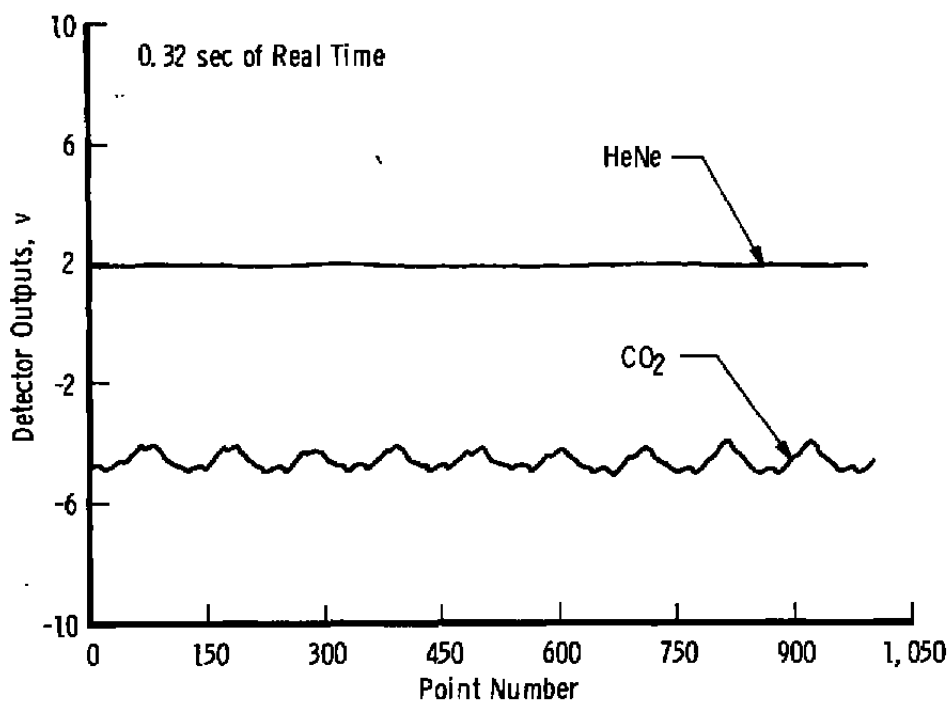
Figure 6. Sample output of detectors during test shot.

where

V is the detector output voltage during the test,

V_O is the detector output voltage with laser beam blocked, and

V_F is the detector output voltage with no attenuation

The instantaneous attenuation data, read from the magnetic tape, were averaged over the recording interval of 0.32 sec to eliminate the effect of random signal noise. These averaged values were used in Eq. (1) to compute experimental values of transmission.

3.3 CHARACTERIZATION OF ATTENUATING MEDIUM

The characterization of the water drops in the attenuation region has been treated in an approximate manner. The number in the region, their size, and approximate geometric locations can be determined. A major uncertainty is the appropriate attenuation area for adjacent drops with overlapping cross-sectional areas.

The transmission through an attenuation region can be expressed as

$$T = 1 - A_E / A_L \tag{2}$$

where A_L is the cross-sectional area of the laser beam and A_E is an extinction area attributable to the attenuating effects of the medium on the laser beam. The extinction area is related to the cross-sectional area the water drops present to the beam by an extinction efficiency, Q_E,

$$A_E = Q_E \sum_{i=1}^{N} A_i \tag{3}$$

where A_i is the effective cross-sectional area of the ith particle and N is the total number of particles in the laser beam. The problem is to determine the individual drop contributions, A_i, from the trajectory measurements, flow rate, and drop formation frequency.

The time interval between drops is given by

$$t_d = 1/f \tag{4}$$

where f is the drop formation frequency. The drop diameter, d, is given by

$$d = \sqrt[3]{\frac{6Q}{\pi f}} \tag{5}$$

with the volumetric flow rate denoted by Q. The number of drops in the attenuation region is given by

$$N = 2f \sqrt{\frac{2h}{g}}$$

(6)

with the maximum drop trajectory height into the beam given by h.

For the special case in which the drops are well separated so that no interactions need be considered, the effective cross-sectional area would be given by

$$\sum_{i=1}^{N} A_i = N \frac{\pi d^2}{4}$$

(7)

In the present case, overlapping area between adjacent drops must be taken into account. When all drops follow a common trajectory, the vertical spacing between adjacent drop centers is given by

$$h_d = t_d \left[V_v - \frac{g}{2} (2t - t_d) \right]$$

(8)

with the initial vertical velocity given by V_v and the time after injection of the drop into the beam given by t. For a common trajectory, the extent of the overlapping areas between adjacent drops can be determined by Eq. (8). The result of the calculation of the overlap area between adjacent drops is shown in **Fig. 7**.

The horizontal extent of the drop trajectory in the laser beam is denoted by L in **Fig. 3**. Experimentally, for each test a certain amount of jitter was found; therefore, the dimension L is an average distance over which the drops remain in the laser beam. The jitter in this dimension was used to estimate the magnitude of the random drop-to-drop dispersion from the mean trajectory. This scatter must be considered in the analysis procedure, since it enters into the calculation of the overlapping area between adjacent drops.

The jitter is assumed to be caused a random variation in the initial velocity of the water drops entering the laser beams. Under this assumption, the fractional variation in L is twice the fractional variation in the initial velocity, and the random component in the vertical drop position is expressed as

$$\delta y = \frac{V_v}{2} \frac{(\delta L)}{L} t$$

(9)

$$A_0 = 2\left[\frac{d^2}{4}\cos^{-1}\left(\frac{h_d}{d}\right) - \frac{h_d}{4}\sqrt{d^2 - h_d^2}\right]$$
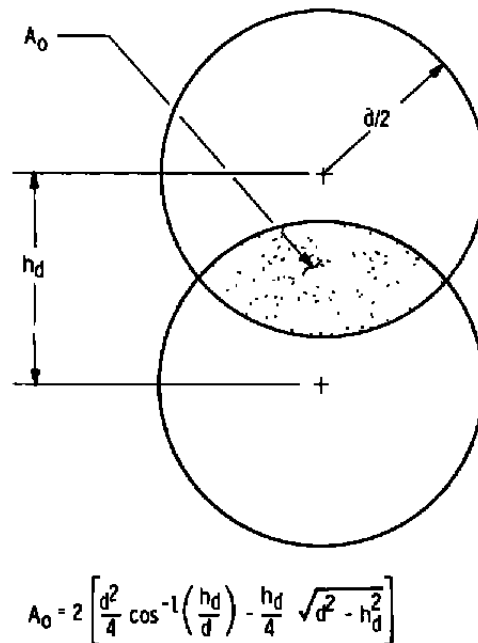
Figure 7. Calculation of overlapping projected area of adjacent drops.

where δL is the extent of the variation in L, V_v is the mean initial vertical drop velocity, and t is the time-of-flight of the drop.

A comparable spread in the horizontal location of the drops perpendicular to the laser beams is also present. Equation (9) also estimates the extent of the horizontal jitter of the individual drops with respect to the vertical plane of the main trajectory.

The projected cross-sectional area of the water drops has been calculated for each test in the following manner. The first drop is assumed to be centered on the border of the laser beam. Half of its area is counted as being in the laser beam. The vertical location of the next drop is then calculated by assuming that it moves along the mean trajectory for a drop formation time. Equation (9) then establishes a maximum deviation from the mean trajectory likely to occur. A uniformly distributed random number between 0 and δy as given by Eq. (9) is taken to be the magnitude of the deviation in position from the mean trajectory. Another uniformly distributed random number between 0 and 2π denotes the direction of the deviation from the mean trajectory. This quantity is added vectorally to the vertical spacing calculated for the mean trajectory to give the separation of the adjacent drops. The area of the second drop is added to the contribution of the first and the overlap area (if overlap exists) is subtracted from the accumulated area. The overlap area is calculated as shown in Fig. 7, with the calculated drop separation distance used as h_d.

The contribution of the next drop to the accumulated area is then considered in a like manner, until the last drop considered falls out of the laser beam. This calculation gives the total number of drops in the laser beams and the appropriate total cross-sectional area occupied by the water drops.

3.4 TRANSMISSION PREDICTIONS

The experimental results have been analyzed using the simplified approximate approach presented in Ref. 1. A sphere placed in a light beam is assumed to interact with the incident radiation in the same manner as an opaque disk of the same diameter. The first effect is that all the radiation intercepted by the disk is blocked. By Babinet's principle (Ref. 2) a like amount of radiation is diffracted from the rim of the disk. Thus, the incident radiation on a circular region of diameter $\sqrt{2}d$ is scattered from its original path by the presence of a disk or sphere of diameter d.

For absorbing spheres with sufficiently large size parameters, i.e. (Ref. 3),

$$x = \pi d / \lambda \geq 2000$$

the scattered radiation intensity distribution can be analyzed using diffraction theory. However, for small scattering angles, diffraction theory appears to approach the results of the much more elaborate Mie scattering theory for values of x as small as 80 (Ref. 4). For the present experiments, $80 < x < 4000$, with scattering angles of interest of less than a degree. Therefore, diffraction theory should be appropriate to the present experimental conditions.

The power received by the detector with no intervening water drops is

$$P_o = I_o A_l \tag{10}$$

with the incident radiation intensity at the attenuation region given by I_o and the cross-sectional area of the laser beams at the region denoted by A_L. When a water drop occupies the attenuation region, the power received by the detector is

$$P = I_o A_L - Q_s I_o A_p + \frac{Q_s}{2} \left(\frac{A_p}{A_L}\right) I_o \int_{A_d} \left(\frac{I_s}{I_o}\right) dA_d \tag{11}$$

where A_p is the cross-sectional area of a water drop, A_d is the cross-sectional area of the detector, and I_s is the scattered radiation intensity. The scattering efficiency of the drop is denoted by Q_s. The first contribution to the power received by the detector in Eq. (11) is that

14

attributable to the power incident on the attenuation region. The second term represents the power scattered by the water drop, and the third term represents the scattered power that is diverted toward the detector.

The scattering efficiency, Q_s, has been evaluated using Eq. (12), which has been taken from Ref. 4:

$$Q_s = 2 - \frac{4}{\rho} \sin \rho + \frac{4}{\rho^2} (1 - \cos \rho) \tag{12}$$

where

$$\rho = \frac{2\pi d}{\lambda} (m - 1) \tag{13}$$

The particle diameter is d, the radiation wavelength is λ, and m is the refractive index of the water drop (taken to be 1.33).

Equations (12) and (13) have been evaluated for the range of the test parameters. The results are shown in Fig. 8 as the envelope of a rapidly oscillating function of particle diameter.

The transmission, T, is given by Eq. (14):

$$T = \frac{P}{P_o} = 1 - Q_s \frac{A_p}{A_L} + \frac{Q_s}{2} \left(\frac{A_p}{A_L}\right) \frac{1}{A_L} \int_{A_d} \left(\frac{I_s}{I_o}\right) dA_d \tag{14}$$

The power scattered in the direction of the detector can be evaluated using Fraünhofer diffraction theory (Ref. 3):

$$I_s / I_o = \left(\frac{\lambda}{2\pi\ell}\right)^2 i(x,\theta) \tag{15}$$

where $i(x,\theta)$ is the Fraünhofer intensity function, θ is the scattering angle, ℓ is the distance from the scattering particle to the detector, and

$$x = \pi d / \pi \tag{16}$$
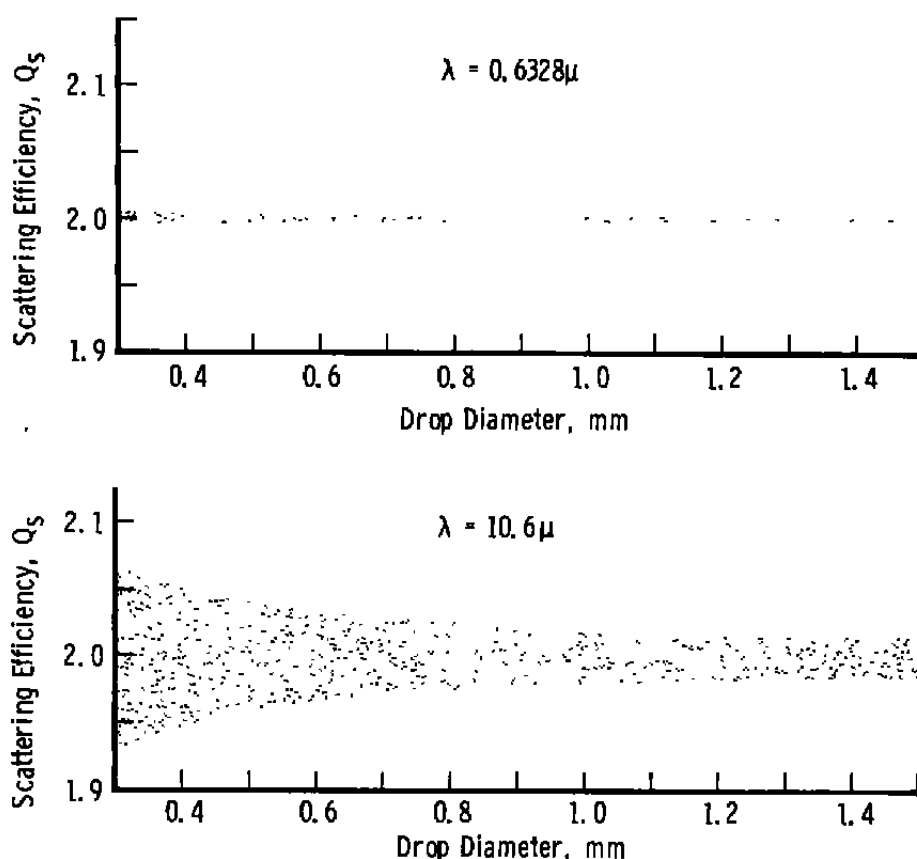
Figure 8. Envelope of scattering efficiencies calculated from Eq. (12).

The intensity function, $i(x,\theta)$ is given by (Ref. 2)

$$i(x,\theta) = x^4 \left[\frac{J_1 (x \sin \theta)}{x \sin \theta} \right]^2 \qquad (17)$$

Values of the intensity function for the region of interest are tabulated in Tables 1 and 2. The zeros of the intensity function occur at values of $x \sin \theta$, which correspond to the roots of J_1, the first order Bessel function. For experiments at either laser wavelength, the angular extent of the detector is less than the scattering angle corresponding to the first root of J_1.

The intensity function must be integrated over the area subtended by the detector to evaluate the fraction of the scattered radiation that is scattered in the direction of the detector. Using ℓ for the distance from the attenuation region to the detector, d_d for the

16

detector diameter, and d_L for the laser beam diameter, the integral of the intensity function can be expressed as

$$\frac{1}{A_L}\int_{A_1}\left(I_s - I_o\right)dA = \frac{2}{x^2}\left(\frac{d}{d_L}\right)^2 \int_o^{\tan^{-1}\left(d_d/2L\right)} i(x,\theta)\frac{\tan\theta}{\cos^2\theta}d\theta \tag{18}$$

The results from Eq. (18) are shown in Fig. 9 for both wavelengths and the range of particle diameters covered by the present tests. The results show that for a wavelength of 10.6 μm, very little radiation is scattered toward the detector, whereas for the HeNe laser beam a considerably larger fraction of the energy is directed toward the detector.

Table 1. Fraünhofer Intensity Functions, $\lambda = 0.6328\ \mu$

Angle, deg

Diameter, mm	0	0.0065	0.0130	0.0195	0.0260
0.3	1.2302×10^{12}	1.2214×10^{12}	1.1954×10^{12}	1.1532×10^{12}	1.0962×10^{12}
0.4	3.8879×10^{12}	3.8388×10^{12}	3.6947×10^{12}	3.4645×10^{12}	3.1623×10^{12}
0.5	9.4919×10^{12}	9.3053×10^{12}	8.7636×10^{12}	7.9191×10^{12}	6.8508×10^{12}
0.6	1.9682×10^{13}	1.9127×10^{13}	1.7539×10^{13}	1.5135×10^{13}	1.2233×10^{13}
0.7	3.6464×10^{13}	3.5070×10^{13}	3.1150×10^{13}	2.5426×10^{13}	1.8889×10^{13}
0.8	6.2206×10^{13}	5.9115×10^{13}	5.0597×10^{13}	3.8661×10^{13}	2.5908×10^{13}
0.9	9.9642×10^{13}	9.3411×10^{13}	7.6623×10^{13}	5.4194×10^{13}	3.2031×10^{13}
1.0	1.5187×10^{14}	1.4022×10^{14}	1.0961×10^{14}	7.0877×10^{13}	3.5933×10^{13}
1.1	2.2235×10^{14}	2.0185×10^{14}	1.4950×10^{14}	8.7153×10^{13}	3.6558×10^{13}
1.2	3.1492×10^{14}	2.8062×10^{14}	1.9572×10^{14}	1.0124×10^{14}	3.3452×10^{13}
1.3	4.3376×10^{14}	3.7877×10^{14}	2.4716×10^{14}	1.1135×10^{14}	2.6976×10^{13}
1.4	5.8343×10^{14}	4.9841×10^{14}	3.0222×10^{14}	1.1599×10^{14}	1.8354×10^{13}
1.5	7.6884×10^{14}	6.4144×10^{14}	3.5882×10^{14}	1.1420×10^{14}	9.5035×10^{12}

Table 2. Fraünhofer Intensity Functions, λ = 10.6 μ

Angle, deg

| Diameter, mm	0	0.0065	0.0130	0.0195	0.0260
0.3	1.5624×10^7	1.5624×10^7	1.5623×10^7	1.5621×10^7	1.5618×10^7
0.4	4.9381×10^7	4.9378×10^7	4.9372×10^7	4.9360×10^7	4.9345×10^7
0.5	1.2056×10^8	1.2055×10^8	1.2052×10^8	1.2048×10^8	1.2042×10^8
0.6	2.4999×10^8	2.4996×10^8	2.4989×10^8	2.4976×10^8	2.4958×10^8
0.7	4.6314×10^8	4.6307×10^8	4.6288×10^8	4.6256×10^8	4.6211×10^8
0.8	7.9001×10^8	7.8995×10^8	7.8952×10^8	7.8880×10^8	7.8781×10^8
0.9	1.2656×10^9	1.2653×10^9	1.2644×10^9	1.2630×10^9	1.2609×10^9
1.0	1.9289×10^9	1.9284×10^9	1.9267×10^9	1.9240×10^9	1.9202×10^9
1.1	2.8241×10^9	2.8232×10^9	2.8203×10^9	2.8155×10^9	2.8087×10^9
1.2	3.9999×10^9	3.9982×10^9	3.9933×10^9	3.9852×10^9	3.9739×10^9
1.3	5.5092×10^9	5.5066×10^9	5.4987×10^9	5.4856×10^9	5.4672×10^9
1.4	7.4102×10^9	7.4061×10^9	7.3938×10^9	7.3733×10^9	7.3447×10^9
1.5	9.7652×10^9	9.7590×10^9	9.7404×10^9	9.7094×10^9	9.6663×10^9
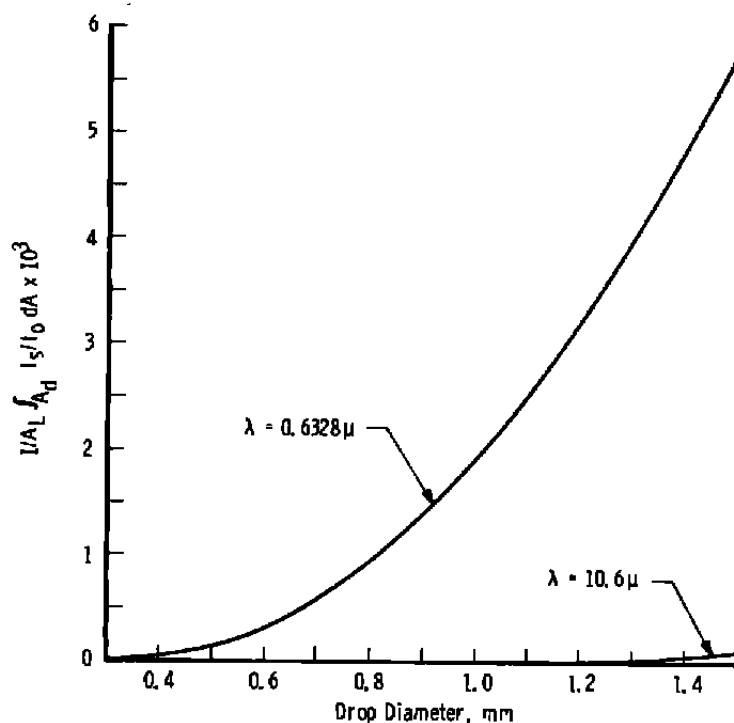
Figure 9. Contribution of forward-scattered radiation to detector signal.

3.5 UNCERTAINTY ESTIMATES

The independently measured quantities along with their estimated uncertainties are listed in Table 3. The assigned uncertainties are based on calibration data and experience and represent an estimated standard deviation of the measured value from the true value of the quantity. The independent quantities can be separated into those that affect the predicted transmissions and those that influence the measured transmissions. This separation is made in Table 3.

Table 3. Estimates of Uncertainty in Measured Quantities

A. Quantities Affecting Predicted Transmission

Symbol	Quantity Description	Estimated Uncertainty
h	Height of water drop trajectory in laser beams	0.05 in.
L	Length of water drop trajectory in laser beams	0.1 in.
Q	Water flow rate	0.01 x Q
f	Frequency of drop formation	0.01 x f
δL	Drop-to-drop variation from mean value of L	0.05 in.

B. Quantities Affecting Measured Values of Transmission

Symbol	Quantity Description	Estimated Uncertainty
V_o	Voltage output of detector with no incident radiation	0.01 v
V_F	Voltage output of detector with no attenuation of incident radiation	0.01 v
V	Voltage output of detector with attenuation of incident radiation	0.01 v

3.5.1 Estimates of Uncertainty in Predicted Transmission

The magnitude of the uncertainty in the predicted transmission can be expressed as

$$\Delta T = \sqrt{\left[\left(\frac{\partial T}{\partial h}\right)\Delta h\right]^2 + \left[\left(\frac{\partial T}{\partial L}\right)\Delta L\right]^2 + \left[\left(\frac{\partial T}{\partial Q}\right)\Delta Q\right]^2 + \left[\left(\frac{\partial T}{\partial f}\right)\Delta f\right]^2 + \left[\left(\frac{\partial T}{\partial \delta L}\right)\Delta \delta L\right]^2}$$

(19)

Calculation of the various terms for a number of sample runs show that the variation of transmission with drop trajectory length, L, is zero. The magnitudes of the other terms are given in Table 4. For the limited number of sample runs considered, the calculated uncertainties in predicted transmission vary from ± 0.0309 to ± 0.0723.

Table 4. Estimates of Uncertainty in Predicted Transmission for Sample Runs

Run No.	$\frac{\partial T}{\partial h} \Delta h$	$\frac{\partial T}{\partial Q} \Delta Q$	$\frac{\partial T}{\partial f} \Delta f$	$\frac{\partial T}{\partial \delta L} \Delta \delta L$	ΔT
10	(-0.26)(0.05)	(-0.000824)(0.607)	(-0.000137)(7.31)	(-0.560)(0.05)	±0.0309
20	(-0.190)(0.05)	(0)(0.273)	(0.0000684)(7.2)	(-0.630)(0.05)	±0.0329
30	(-0.120)(0.05)	(-0.0231)(0.065)	(0)(52.2)	(-1.44)(0.05)	±0.0723
40	(-0.230)(0.05)	(-0.224)(0.0647)	(-0.000269)(50.2)	(-0.83)(.05)	±0.0474

3.5.2 Estimates of Uncertainty in Measured Transmission

The measured transmission has been given by Eq. (1). The uncertainty in measured transmission is given by

$$\Delta T = \sqrt{\left[\left(\frac{\partial T}{\partial V}\right)\Delta V\right]^2 + \left[\left(\frac{\partial T}{\partial V_o}\right)\Delta V_o\right]^2 + \left[\left(\frac{\partial T}{\partial V_F}\right)\Delta V_F\right]^2} \quad (20)$$

And from Eq. (1),

$$\frac{\partial T}{\partial V} = \frac{1}{V_F - V_o} \quad (21)$$

$$\frac{\partial T}{\partial V_o} = \frac{V - V_F}{\left(V_F - V_o\right)^2} \quad (22)$$

$$\frac{\partial T}{\partial V_F} = \frac{V_o - V}{\left(V_F - V_o\right)^2} \quad (23)$$

Uncertainties in measured transmission have been assessed using an uncertainty of 0.01 for all voltages and Eqs. (21) through (23) in Eq. (20). The results are tabulated in Table 5 for the sample cases considered. For the HeNe laser, $0.00167 \leq \Delta T \leq 0.00261$, and for the CO_2 laser, the uncertainty is $0.00170 \leq \Delta T \leq 0.00469$. These values are small compared to the uncertainties in predicted transmission. The major source of the data uncertainty, from the uncertainty analysis, is the characterization of the attenuating medium. The effective cross-sectional area of the water drops is the least well-defined parameter and the drop-to-drop jitter in the trajectory is the major source of this possible error.

Table 5. Estimates of Uncertainty in Measured Transmission for Sample Runs

	Run No.							
	10		20		30		40	
	HeNe	CO_2	HeNe	CO_2	HeNe	CO_2	HeNe	CO_2
$\partial T/\partial V$	0.1317	0.1572	0.2014	0.1678	0.1661	0.3421	0.1696	0.3106
$\partial T/\partial V_o$	−0.03489	−0.02275	−0.03964	−0.01934	−0.02129	−0.02270	−0.02631	−0.02785
$\partial T/\partial V_F$	−0.09676	−0.1345	−0.1618	−0.01484	−0.1448	−0.3194	−0.1433	−0.2828
ΔT	±0.00167	±0.00208	∓0.00261	±0.00170	±0.00221	±0.00469	±0.00224	±0.00421

4.0 RESULTS

The transmission, given by Eq. (14), has been calculated for each test run, using Eqs. (17) and (18) to evaluate the contribution of the scattering by the particles. The results are tabulated in Table 6, along with the experimental transmission measurements. The drop diameter has been calculated for each test using Eq. (5), and the total number of drops in the laser beam has been computed using Eq. (6). The appropriate total projected area of the drops in the beam has been calculated for each test run assuming interactions only between adjacent drops as previously described.

For the HeNe laser Fig. 10 compares the predicted values obtained from Eq. (14) with the experimental transmission measurements on each test. Figure 11 gives the corresponding comparisons for the CO_2 laser. The standard deviation of the measured data from the predicted values is also included in Figs. 10 and 11. Figure 12 compares the experimental transmission of the HeNe laser beam with the experimental transmission of the CO_2 laser beam while both are attenuated by a common water drop field. With the exception of a couple of points, the agreement is within about 10 percent.

Table 6. Tabulated Test Results

Run No.	Drop Diameter, mm	Total No. of Drops	Total Drop Area, cm^2	Calculated Transmission		Measured Transmission	
				HeNe	CO$_2$	HeNe	CO$_2$
1	1.420	74	0.994	0.609	0.611	0.646	0.601
2	1.428	74	0.477	0.812	0.812	0.743	0.834
3	1.426	81	0.523	0.794	0.795	0.781	0.767
4	1.427	74	0.452	0.822	0.822	0.815	0.806
5	1.429	66	0.458	0.820	0.819	0.745	0.870
6	1.435	87	0.606	0.761	0.759	0.782	0.741
7	1.367	100	0.587	0.769	0.768	0.800	0.794
8	1.373	92	0.510	0.799	0.797	0.826	0.908
9	1.373	92	0.510	0.799	0.797	0.818	0.778
10	1.383	92	0.516	0.797	0.797	0.856	0.751
11	1.355	105	0.581	0.771	0.772	0.816	0.701
12	1.369	129	0.826	0.675	0.672	0.772	0.705
13	1.023	77	0.594	0.766	0.764	0.738	0.735
14	1.011	82	0.523	0.794	0.794	0.794	0.815
15	1.049	127	0.613	0.758	0.756	0.866	0.964
16	1.053	108	0.490	0.807	0.805	0.909	0.746
17	1.054	108	0.490	0.807	0.805	0.911	0.855
18	1.054	108	0.490	0.807	0.805	0.733	0.987
19	1.038	80	0.619	0.756	0.758	0.718	0.807
20	1.065	97	0.439	0.827	0.828	0.884	0.806
21	1.029	89	0.542	0.786	0.787	0.343	0.824
22	1.041	111	0.581	0.771	0.772	0.845	0.732
23	1.045	111	0.490	0.807	0.806	0.946	0.800
24	0.338	768	0.406	0.840	0.839	0.841	0.845
25	0.326	589	0.452	0.822	0.826	0.887	0.759

Table 6. Concluded

| Run No.	Drop Diameter, mm	Total No. of Drops	Total Drop Area, cm^2	Calculated Transmission		Measured Transmission	
				HeNe	CO$_2$	HeNe	CO$_2$
26	0.328	592	0.426	0.832	0.837	0.889	0.768
27	0.325	808	0.142	0.944	0.945	0.998	0.976
28	0.337	672	0.413	0.837	0.837	0.778	0.923
29	0.340	581	0.265	0.896	0.894	0.869	0.913
30	0.341	651	0.1742	0.931	0.930	0.928	0.879
31	0.331	560	0.361	0.857	0.861	0.907	0.824
32	0.350	458	0.406	0.840	0.837	0.929	0.702
33	0.346	479	0.265	0.896	0.892	0.837	0.951
34	0.340	655	0.129	0.949	0.948	0.949	0.979
35	0.334	550	0.381	0.850	0.852	0.878	0.830
36	0.323	601	0.252	0.901	0.902	0.897	0.884
37	0.323	601	0.174	0.931	0.932	0.901	0.949
38	0.326	494	0.116	0.954	0.955	0.996	0.902
39	0.342	511	0.161	0.936	0.935	0.882	0.896
40	0.345	542	0.290	0.885	0.882	0.904	0.853
41	0.350	489	0.181	0.929	0.927	0.934	0.894
42	0.343	636	0.129	0.949	0.948	0.920	0.985
43	0.320	1047	0.310	0.878	0.877	0.863	0.875
44	0.336	863	0.355	0.860	0.861	0.864	0.900
45	0.343	466	0.097	0.962	0.961	0.972	0.936
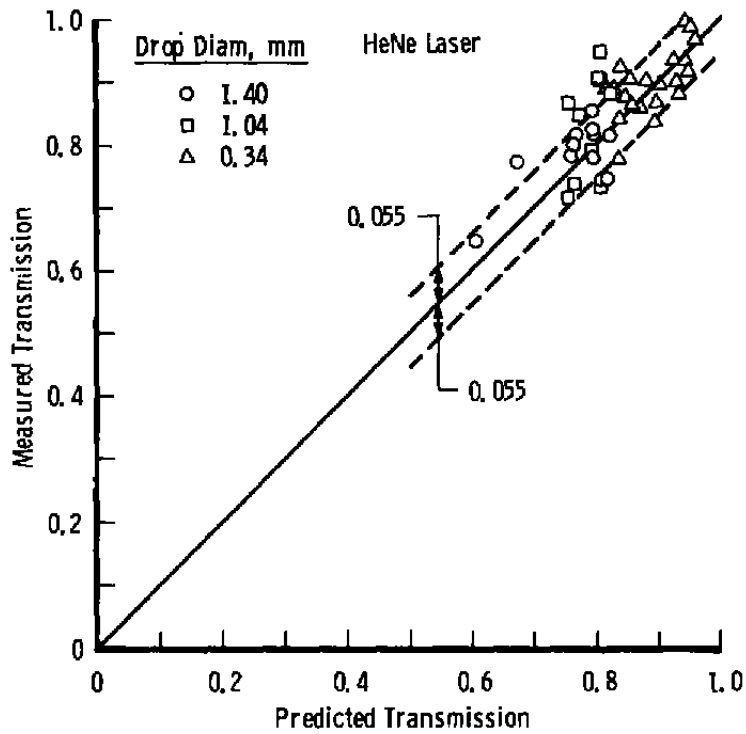
Figure 10. Comparison of measured and predicted transmission, $\lambda = 0.6328\ \mu$.
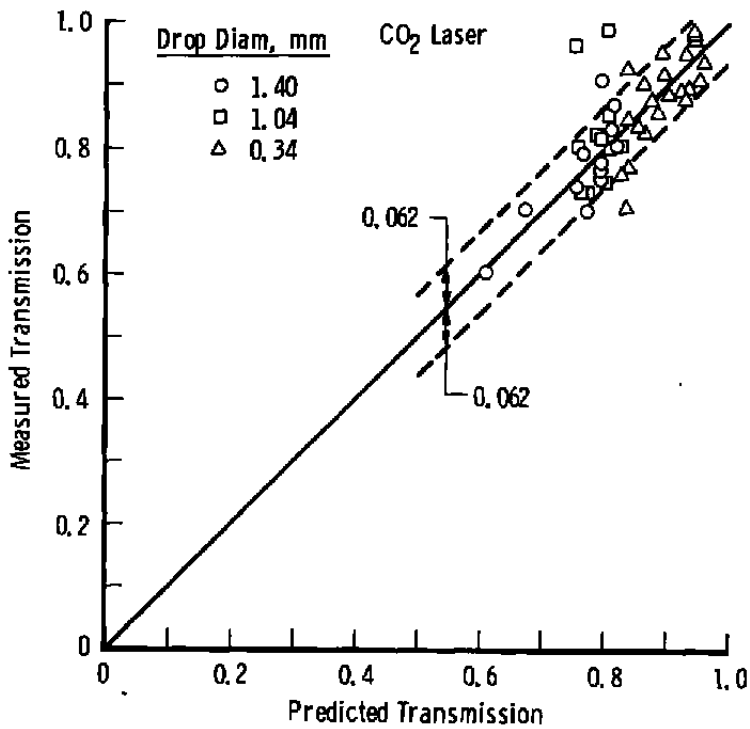

Figure 11. Comparison of measured and predicted transmission, $\lambda = 10.6\ \mu$.
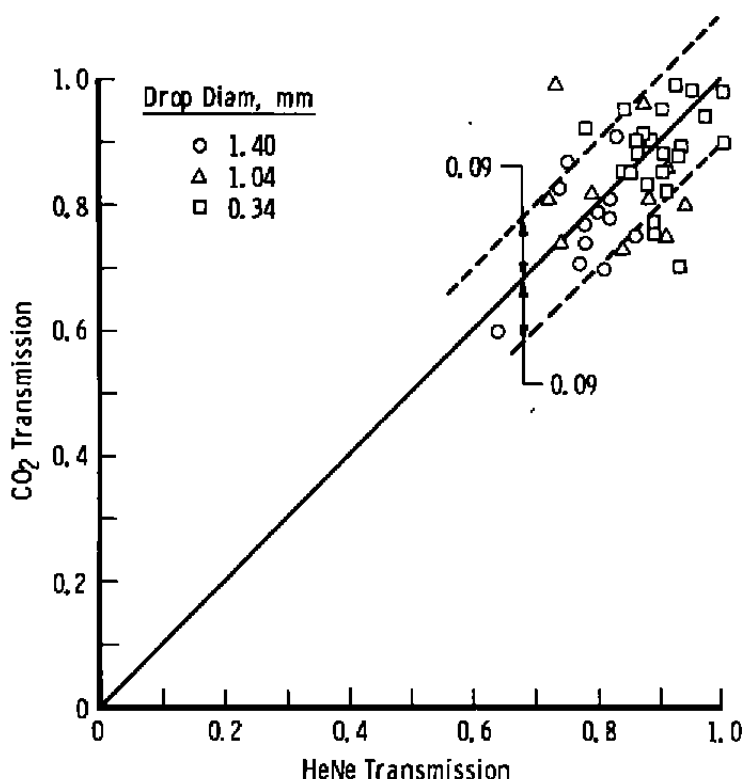
Figure 12. Comparisons of transmission measurements for HeNe and CO$_2$ lasers.

5.0 SUMMARY AND CONCLUSIONS

The transmission of a HeNe laser beam and a coincident CO$_2$ laser beam through a stream of uniformly sized water drops were simultaneously measured. The detector outputs were digitized online with a thousand data points on each channel recorded for a duration of 0.3 sec. These signals were averaged over the time interval to remove any transient effects. The online transmission data were processed by computer to give measured transmission data.

The attenuation environment was characterized by various measurements from which the drop diameter, effective drop cross-sectional area, and number of drops in the laser beams could be determined. Drop sizes ranged from 0.3 mm up to 1.4 mm in diameter.

Fraunhofer diffraction theory was used to predict the experimental results. The attenuation effect of a single water drop was calculated from simple diffraction theory. This effect was converted into an extinction efficiency, and the extinction efficiency was in turn multiplied by the total effective cross-sectional area occupied by the drops to yield a predicted attenuation for each test run.

Comparisons between the measured and predicted transmissions show satisfactory agreement. The magnitude of the deviation of the predicted transmission from the experimental transmission is the same as would be expected from the uncertainty in the quantification of the attenuating medium. Within the limits imposed by the experimental technique, simple diffraction theory adequately predicts the experimental results.

It is concluded that the major source of uncertainty in laser attenuation measurements is the definition of the attenuating medium. To make more definitive attenuation measurements, a better defined attenuating medium is required. The ability to place more particles in the attenuation region would also be desirable.

REFERENCES

1. Kerker, Milton. *The Scattering of Light, and Other Electromagnetic Radiation.* Academic Press, New York and London, 1969, pp. 106, 107.

2. Condon, E. U. and Odishaw, Hugh, editors. *Handbook of Physics.* McGraw-Hill Book Company, New York, Toronto, and London, 1958, pp. 6-79, 6-82.

3. Dave, J. V. "Scattering of Visible Light by Water Spheres." *Applied Optics,* Vol. 8, No. 1, January 1969, pp. 155-164.

4. von de Hulst, H. E. *Light Scattering by Small Particles.* John Wiley & Sons, New York, 1957, p. 176.

NOMENCLATURE

A_d Cross-sectional area of detector

A_E Extinction area

A_i Effective cross-sectional area of the ith drop

A_L Cross-sectional area of laser beam at attenuation region

A_o Overlap area between adjacent drops

A_p Cross-sectional area of scattering particle

d   Drop diameter

d_d Diameter of detector

d_L Diameter of laser beam in attenuation region

f   Frequency of drop formation

g   Acceleration of gravity

h   Height of drop trajectory in laser beam

h_d Vertical spacing between adjacent drops

I_o Power per unit area incident on attenuation region

I_s Power per unit area scattered by particle

$i(x,\theta)$ Fraunhofer intensity function

L   Length of drop trajectory in laser beam

m   Index of refraction of particle

N   Total number of water drops in laser beam

27

P	Power incident on detector
P_0	Power incident on detector with no attenuation
Q	Volumetric flow rate of water to drop generator
Q_E	Extinction efficiency
Q_s	Scattering efficiency
T	Transmission
t	Time counted from entry of drop into laser beam
t_d	Time internal between formation of successive drops
V	Detector output voltage during test
V_F	Detector output voltage with no attenuation
V_v	Initial vertical velocity of water drop
v_0	Detector output voltage with laser beam blocked
x	Size parameter ($x = \pi d/\lambda$)
δL	Magnitude of drop-to-drop variation in trajectory length in laser beam
δy	Random component of vertical drop position
θ	Angle between laser beam axis and point on detector, viewed from attenuation region
λ	Laser wavelength
ϱ	Function of size parameter and index of refraction of particle